Chapter 5

A Measuring Approach to Assess the Corrosion Rate of Magnesium Alloys Using Electrochemical Impedance Spectroscopy

Maria C. Delgado, Federico R. García-Galvan,
Violeta Barranco and Sebastian Feliu Batlle

Additional information is available at the end of the chapter

http://dx.doi.org/10.5772/65018

Abstract

An attempt was made to estimate the corrosion rate of AZ31 and AZ61 magnesium alloys immersed in 0.6 M NaCl during long-term exposure using electrochemical impedance spectroscopy (EIS). The EIS results were compared with the corrosion rate independently assessed by the hydrogen evolution test. A correlation was established between the integration of the polarization resistance (R_p) and charge transfer resistance (R_t) over time, as evaluated by EIS and hydrogen gas measurements. Regardless of the immersion time, a strong link was found between the R_t and R_p values determined by EIS. This relation seems to depend on the composition of the alloy. The influence of immersion time on the estimated corrosion rate reliability was investigated. The typical deviations of the measurement methods are apparently decreasing upon prolonging the immersion time. No significant errors were obtained in the measurement of the corrosion rate when using R_t or R_p determined by EIS with their corresponding "apparent" Stern-Geary coefficient values compared with the real values determined by gravimetric measurements.

Keywords: Magnesium, weight loss, electrochemical impedance spectroscopy, corrosion rate, hydrogen evolution

1. Introduction

Mg-Al alloys have aroused great scientific and technological interest in recent decades. From a practical point of view, their high strength-weight ratio makes them ideal alloys for automotive,

aerospace and electronics applications, where weight reduction is of significant concern [1]. The usage of magnesium alloys in automotive applications can significantly contribute to greater fuel savings and environmental conservation [2]. Also, magnesium and its alloys have been investigated recently by many authors as a suitable biodegradable biomaterial [3]. However, their corrosion performance at the current stage of development is still not good enough for increasingly diverse their practical applications [4]. Given the growing use of Mg alloys as structural alloys, an accurate assessment of corrosion is imperative and the unambiguous determination of electrode kinetics in the case of Mg electrodes is essential [5].

Electrochemical impedance spectroscopy (EIS) has been shown in innumerable studies to be an efficient and accurate tool for investigating the nature of surface films and the associated corrosion mechanisms of metals and alloys [6]. The most outstanding and well-known advantages of EIS are that it allows continuous monitoring of the corrosion with measurements of the instantaneous corrosion rate. Such measurements of the corrosion rate require only minor disturbance in the system because a very small AC signal is applied [7]. The use of electrochemical impedance spectroscopy (EIS) to assess electrochemical corrosion behavior of magnesium and its alloys is of great technical relevance. Since stationary values take significant time to become established, it should be noted that short-term measurements may give rise to misleading comparisons of corrodibility of the magnesium alloys [8]. As James et al. [9] noted, EIS is an ideal method for monitoring the long-term corrosion behavior and ranking the corrosion protective ability of Mg and its alloys. The term "long term" is used to distinguish it from the standard electrochemical corrosion studies, which are performed within the first 1 or 2 h [9].

Many Mg corrosion studies assign the first capacitive semicircle, appearing at high frequencies, to the charge transfer reaction of Mg-Al alloys with a partial protective oxide/hydroxide layer formed as the corrosion product in the test solution [6, 9–14]. The charge transfer resistance R_t is determined by the diameter of this capacitive loops [15–20]. The corrosion rate of freely corroding metal in the absence of coverage effects is inversely proportional to polarization resistance as described by the Stern-Geary relationship [21, 22]:

$$i_{corr} = \frac{\mathrm{B}}{R_t} \tag{1}$$

where B is the Stern-Geary constant and can be determined using anodic (β_a) and cathodic (β_c) Tafel slopes [23] ($B = (1/2.303) \times (\beta_a.\beta_c/(\beta_a+\beta_c))$.

The determination of the anodic Tafel slope is not trivial because the magnesium electrode can sustain very high anodic current with minimal anodic polarization, accompanied by substantial hydrogen evolution and local alkalinization, producing a large Ohmic drop in the proximity of the electrode surface [24]. Anodic potentiodynamic polarization of Mg and Mg alloys initially exhibits a very low apparent Tafel slope, representative of an ideally non-polarizable electrode behavior, followed by the bending of the curve [22, 24–26].

http://dx.doi.org/10.5772/65018

In our previous studies [15, 19, 20], due to the uncertainty in the β_a values from the polarization curves commented above [22, 24–26], it was decided to use the constant B estimated empirically from the correlation between electrochemical and gravimetric measurements [15]. Previous investigation [27] yielded B values of around 65 mV for the AZ31 alloy and of around 120 mV for the AZ61 alloy. Cumulative weight loss after an extended period of time was determined by the integration of the weight changes for individual exposure periods. In this way, the average corrosion rates of the specimens after 14 days of exposure to the 0.6 M NaCl solution were obtained from EIS, which were similar to that determined from hydrogen evolution and gravimetric measurements [28].

Recently, King et al. [22] and Bland et al. [26] have shown that the determination of polarization resistance, R_p, at the zero frequency limit as evaluated from analysis of impedance data, provided excellent correlation between the volume of hydrogen collected and mass loss, for both commercially pure Mg and the AZ31 alloy. King et al. [22] critically address previous studies which have utilized the impedance behavior of magnesium and which claim electrochemical tests may underestimate the corrosion rate of Mg; in most cases by a factor of 2 or more, while attempting to use a charge transfer resistance at intermediate frequencies and do not account for the electrochemically justified inductive behavior. Later, Curioni et al. [24] have revealed that the reciprocal of the values of resistance estimated by EIS is linearly correlated with the corrosion current measured by hydrogen collection. The experimentally measured proportionality constant provides an "apparent" Stern-Geary coefficient that can be used to evaluate the corrosion current from EIS data [24].

In these studies [22, 24, 25], impedance measurements were taken during free corrosion while monitoring in real time the amount of hydrogen evolved from the corroding electrodes to obtain instantaneous values of corrosion current of pure magnesium and the AZ31 alloy in NaCl solutions. As Curioni et al. [24] commented, the lack of reproducibility of the corrosion current is due to statistical variation in the corrosion process, but the combined measurement of the corrosion rate by impedance spectroscopy and hydrogen evolution is reliable. From a practical viewpoint, however, the possibilities of obtaining "apparent" Stern-Geary coefficients from the relationship between independent hydrogen evolution and electrochemical impedance spectroscopy measurements are of interest since the experimentation is easy to replicate and to implement; although long exposure times may be involved, the relatively simple procedure reduces the propensity to introduce systematic errors.

The effect of exposure time to the corrosive solution is important since there are frequent cases in which the corrosion rate of Mg tends to change significantly with the immersion time [8, 29–34]. Typically, the initial corrosion rate is less, and then the corrosion rate accelerates to a steady state [35–38]. Due to the high protective nature of the pre-existing native oxide film formed on the polished surfaces of some magnesium alloys, significant fractions of uncorroded silvery regions can be found even after 24 h immersion in 3.5% NaCl aqueous solution [29, 32]. Bland et al. [26] noted that because of the rapid corrosion rates normally observed for the Mg system, the Tafel characteristics can change dramatically between a short- and long-term test. Hsieh et al. [39] examined the relationship between weight loss (WL) measurements and polarization resistance measurements of corrosion in metals and metal alloys (mild steel,

aluminum, copper, and cupronickel) commonly used in industrial cooling systems. The experimentally measured proportionality constant *B'*, based on the correlation between electrochemically and gravimetric measured corrosion rates, changes with the exposure time until steady state is reached, which may take up to 3 days. At longer immersion times (>3 days), the *B'* value begins to stabilize and changes little with the corrosivity of water. For this reason, long-term exposure to saline aqueous solutions was selected (AZ31 specimen after 4 days and AZ61 specimen after 14 days of testing) for the measurement of an "apparent" Stern-Geary coefficient for these alloys. The purpose of this study is to report new results within a broader study carried out on the factors affecting the estimation of the corrosion rate in magnesium alloys by EIS [31]. The ultimate aim is to expand our overall understanding of such phenomena and improve the reliability of the experimental results by devising better study designs.

The summary of main results of corrosion rates of pure Mg and magnesium alloys evaluated from electrochemical measurements [5, 16, 17, 22, 24, 26, 32, 38, 40–46] can be seen in **Table 1**.

Authors	Work title	Main aspects	Reference
Makar L, Kruger J	Corrosion Studies of Rapidly Solidified Magnesium Alloys	The charge transfer resistance could be used to accurately measure the corrosion rates of magnesium alloys.	[17]
Kirkland NT, Birbilis N, Staiger MP	Assessing the corrosion of biodegradable magnesium implants: A critical review of current methodologies and their limitations	EIS also does not directly yield a corrosion rate of magnesium implants.	[40]
Pebere N, Riera C, Dabosi F	Investigation of magnesium corrosion in aerated sodium sulfate solution by electro-chemical impedance spectroscopy	The electrochemical determination of the corrosion rate are in agreement with those obtained by atomic absorption spectroscopy.	[16]
Liu M, Schmutz P, Uggowitzer PJ, Song GL, Atrens A	The influence of yttrium (Y) on the corrosion of Mg-Y binary alloys	The corrosion rate evaluated by electrochemical impedance spectroscopy was somewhat smaller than that evaluated from H evolution.	[41]
King AD, Birbilis N, Scully JR	Accurate electrochemical measurement of magnesium corrosion rates; a combined impedance, mass-loss and hydrogen collection study	The determination corrosion rate from EIS polarization resistance correlated to the mass loss and volume of hydrogen collected.	[22]
Qiao ZX, Shi ZM, Hort N, Abidin NIZ, Atrens A	Corrosion behaviour of a nominally high purity Mg ingot produced by permanent mould direct chill casting	The corrosion rate measured using electrochemical techniques was consistently lower than that measured independently by weight loss or hydrogen evolution.	[42]
Bland LG, King AD, Birbilis N, Scully JR.	Assessing the corrosion of commercially pure magnesium	The integration of the polarization resistance over time, as evaluated from EIS provided	[26]

Authors	Work title	Main aspects	Reference
	and commercial AZ31B by electrochemical impedance, mass-loss, hydrogen collection, and inductively coupled plasma optical emission spectrometry solution analysis	correlation to the cumulative mass loss, ICP-OES solution analysis, and volume of hydrogen collected for commercially pure Mg and for AZ31.	
Shkirskiy V, King AD, Gharbi O, Volovitch P, Scully JR, Ogle K, Birbilis N.	Revisiting the electrochemical impedance spectroscopy of magnesium with online inductively coupled plasma atomic emission spectroscopy	In real time, electrochemical impedance spectroscopy (EIS) was coupled with online atomic emission spectroelectrochemistry (AESEC) to simultaneously measure Mg corrosion.	[5]
Curioni M, Scenini F, Monetta T, Bellucci F	Correlation between electrochemical impedance measurements and corrosion rate of magnesium investigated by real-time hydrogen measurement and optical imaging	A very good correlation between values of resistances estimated by EIS and corrosion currents obtained from real-time hydrogen measurement was found.	[24]
Shi ZM, Cao FY, Song GL, Atrens A	Low apparent valence of Mg during corrosion	The values of the corrosion evaluated from EIS data were typically not good measurements of the corrosion rate of Mg as measured by weight loss.	[43]
Atrens A, Song GL, Cao F, Shi Z, Bowen PK.	Advances in Mg corrosion and research suggestions	The reliability of corrosion rate obtained by EIS is questionable.	[38]
Shi ZM, Liu M, Atrens A	Measurement of the corrosion rate of magnesium alloys using Tafel extrapolation	In principle, the electrochemical measurement hypothesis for Mg can be disproved.	[44]
Cao FY, Shi ZM, Hofstetter J, Uggowitzer PJ, Song GL, Liu M, Atrens A.	Corrosion of ultra-high-purity Mg in 3.5% NaCl solution saturated with Mg(OH)(2)	The amount of dissolution under electrochemical control was a small amount of the total dissolution.	[45]
Atrens A, Song GL, Liu M, Shi Z, Cao F, Dargusch MS	Review of recent developments in the field of magnesium corrosion	Good values of the Tafel slopes are needed to EIS measurements of the corrosion rate.	[32]
Frankel GS, Samaniego A, Birbilis N	Evolution of hydrogen at dissolving magnesium surfaces	Cathodic reaction of magnesium is enhanced during dissolution	[46]

Table 1. Summary of previous studies about the estimation the corrosion rate using electrochemical techniques.

2. Materials and methods

AZ31 and AZ61 magnesium alloys manufactured under wrought conditions with the chemical composition indicated in **Table 2** (as detailed by the manufacturer, Magnesium Elektron Company) were used in the present study. Samples were cut into test strips, 2 ×2 cm squares with a thickness of 0.3 cm and then mechanically dry grounded successively with finer and finer abrasive paper up to P2000 SiC grit papers and polished to produce a uniformly flat surface with mirror-like reflectivity. All samples were rinsed in distilled water and dried in air stream as the final step.

Alloy	Al	Zn	Mn	Si	Fe	Ca	Mg
AZ31	3.1	0.73	0.25	0.02	0.005	0.0014	Bal.
AZ61	6.2	0.74	0.23	0.04	0.004	0.0013	Bal.

Table 2. Chemical composition of AZ31 and AZ61 alloys (wt. %).

The corrosion rate of magnesium alloys was calculated from the volume of collected hydrogen during the corrosion test. Specimens were immersed in a beaker containing 700 ml of 0.6 M NaCl. The beaker was covered with an inverted funnel, and the released gas was collected in a graduated burette. All experiments were conducted at room temperature. The hydrogen evolution was measured for 4 days in the case of the AZ31 specimen and for 14 days in the case of the AZ61 specimen. Three replicated specimens were tested to confirm reproducibility of the results. Also, the corrosion rates were determined from the weight loss of the tested specimens, after removing all the corrosion products from the sample surface using chromic acid (200 g L^{-1} CrO_3 + 10 g L^{-1} $AgNO_3$).

Electrochemical experiments were performed using an AUTOLAB PGSTAT30, with a frequency response analyzer. EIS scans were acquired from 100 kHz to 0.005 Hz with 5 points per decade and an AC amplitude of ±10 mV. A three electrode configuration was used in which the sample was the working electrode, a graphite rod was the counter electrode, and an Ag/AgCl (Sat.) electrode was the reference electrode. The tested specimens exposed an area of 9.0 cm^2 to the 0.6 M NaCl solution. Measurements were performed in triplicate to ensure the reproducibility of the results. ZView software was used for equivalent circuit fitting to the impedance plots obtained in these experiments [47].

3. Results and discussion

3.1. Influence of the immersion time on the error margin of the hydrogen evolution and electrochemical impedance measurements in 0.6 M NaCl solution

Figure 1 compares the time evolution of the corrosion current measured by the hydrogen collection method of tested materials immersed in 0.6 M NaCl solution. The corrosion current

http://dx.doi.org/10.5772/65018

for the AZ31 alloy initially increased slowly during the first day of immersion, after which it increased approximately linearly with the immersion time. This can be attributed to an incubation period in which the initial surface films were partially protective and break down, leading to the steady state corrosion indicated by the later linear trend [48]. The AZ31 alloy was completely dissolved after 4 days of immersion. In contrast, for the AZ61 alloy (**Figure 1b**), the corrosion current measured by the hydrogen evolution was relatively small for the whole immersion duration (14 days). This difference may be due to the strong protective effect of the oxide film that forms spontaneously on the polished AZ61 alloy surface, much more perfect and protective than the film on the AZ31 alloy [29, 31, 49]. The absence of significant variations in the corrosion current measured by the hydrogen evolution for the AZ61 alloy (**Figure 1b**) indicates the presence of a very protective film in this case.

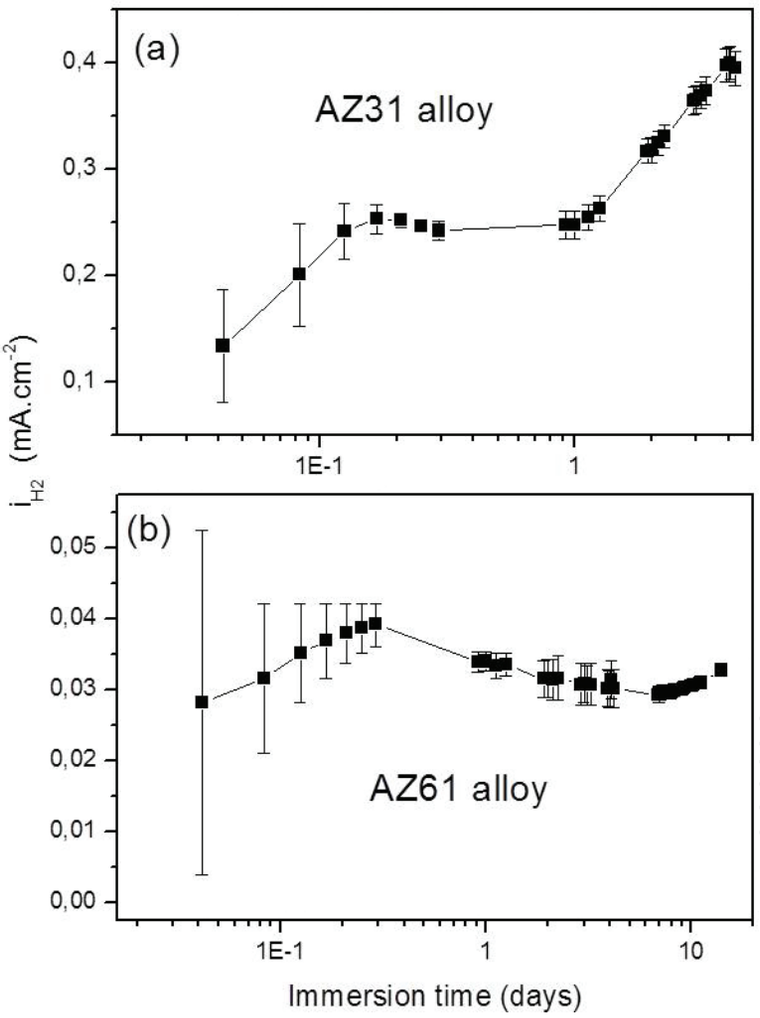

Figure 1. Time evolution of the corrosion current obtained from hydrogen measurement during immersion in 0.6 M NaCl.

Figure 1 also presents the error bars, which indicate the data variability, as deduced from three parallel measurements. It is interesting to note that the error tends to decrease quickly with

immersion time. The observed variations in the error bars-time behavior are attributed to a larger quantity of evolved volume of hydrogen with increasing immersion time, which improves the scale-reading precision [50]. On the other hand, hydrogen gas is very soluble in aqueous environments [22, 51], so it is likely that some H_2 was lost by dissolution in the first stages of experimentation [52].

The Nyquist diagrams (**Figure 2**) obtained for the AZ31 and AZ61 specimens immersed in 0.6 M NaCl show the presence of a capacitive loop at high frequencies (HF) and an inductive loop at low frequencies (LF). **Figure 3** shows the representative impedance spectra of the tested specimens in term of Bode plots.

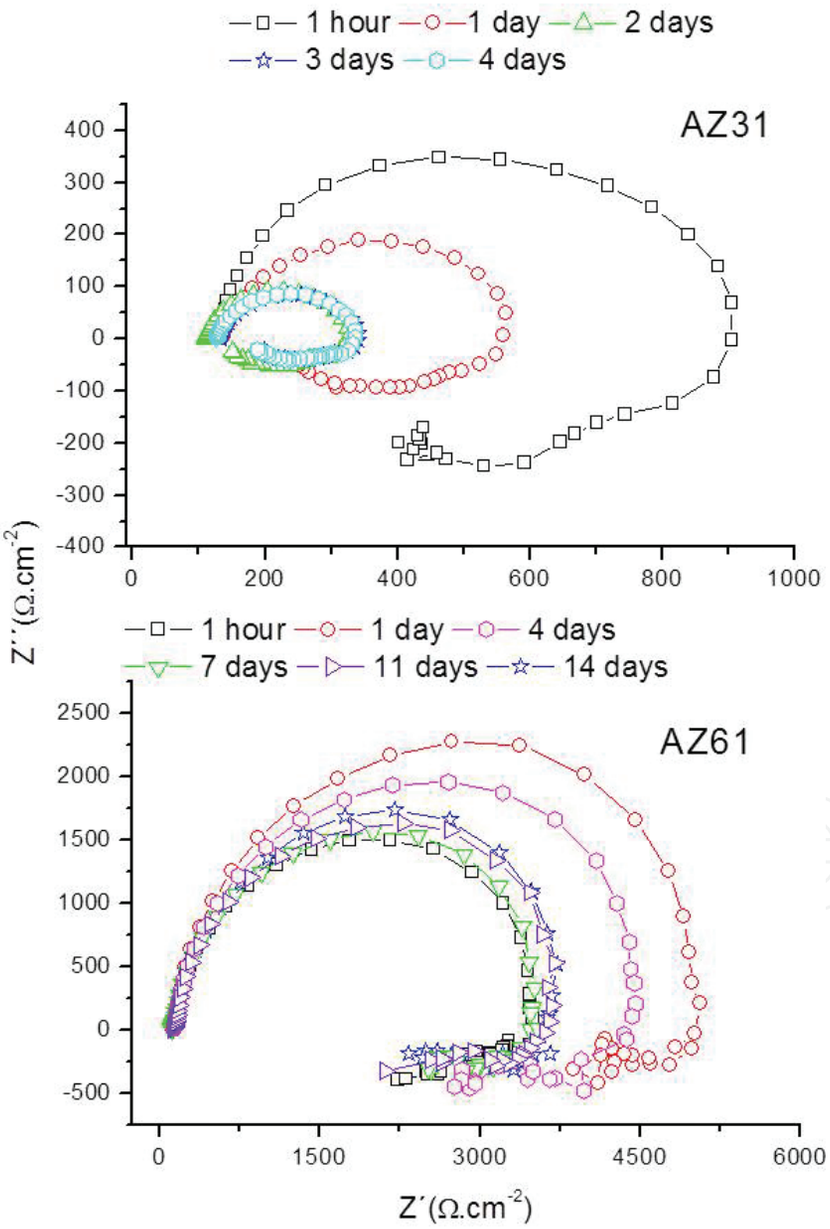

Figure 2. Variation in Nyquist plots for AZ31 and AZ61 samples with immersion time in 0.6 M NaCl solution.

http://dx.doi.org/10.5772/65018

The impedance spectra fitted with the equivalent circuit, as shown in **Figure 4**, were reported by King et al. [22]. R_s represents the electrolyte resistances, C_1 and C_2 are associated with the oxide/hydroxide layers capacitance and the double layer capacitance at the metal/electrolyte interface, respectively. R_1 is related to the initial metallic corrosion step, and R_2 represents the discharge of the intermediate adsorbed species formed in the initial step [53, 54]. Finally, L accounts for the variation in the extension of active anodic regions during the sinusoidal polarization, and R_3 represents the resistances associated with local environmental changes (precipitation of gels, presence of bubbles) nearby the anodic and cathodic regions [24]. In full compliance with the suggestions of King et al. [22], for the analysis of EIS data, in this work, we have included capacitors in the place of constant phase element (CPE) for the representation of the capacitive elements.

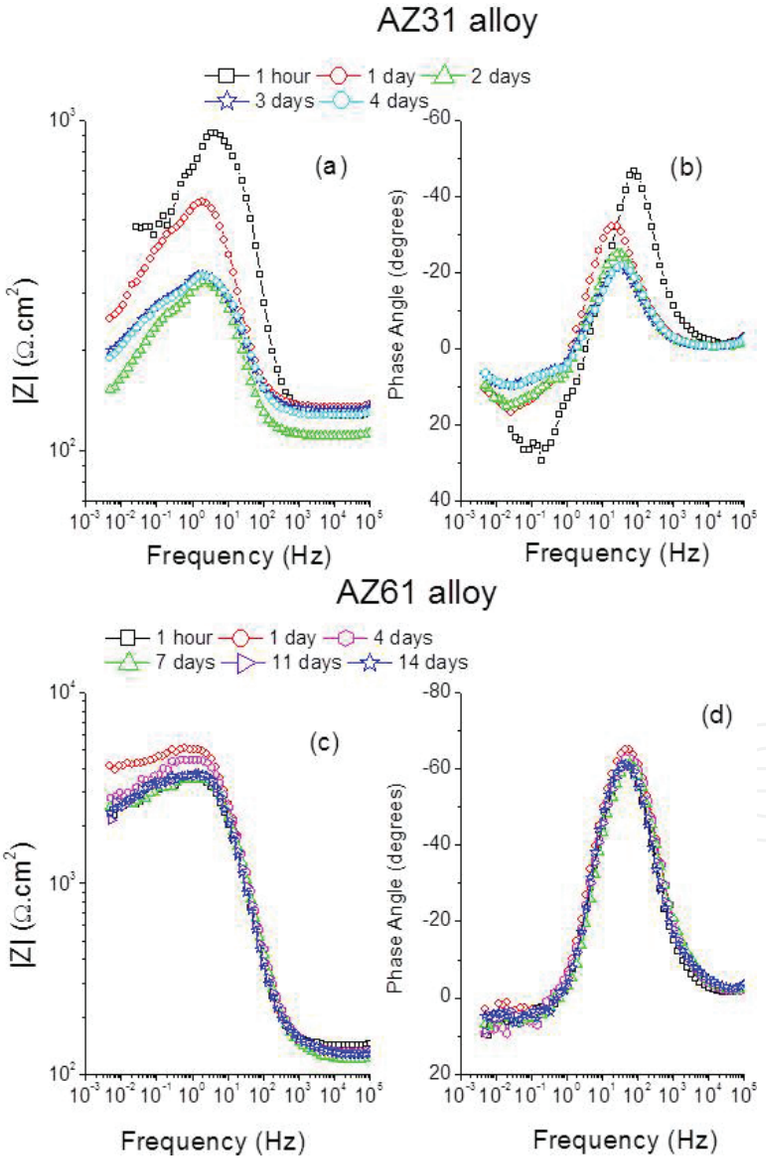

Figure 3. Variation in Bode plots for AZ31 and AZ61 samples with immersion time in 0.6 M NaCl solution.

The Nyquist and Bode plots in **Figure 5** include the measured data along with a fit employing the equivalent circuit proposed and validated by King et al [22]. Generally, the simulated and experimental impedance spectra were closely similar, and the center of the Nyquist plots does not appear depressed, which is a near ideal capacitive behavior [22, 26]. Polarization resistance (R_p) can profile the corrosion rate with time [55]. According to King et al. [22], the R_p can be evaluated as the zero frequency impedance ($f \rightarrow 0$) at $-Z'' = 0$ [56]. On the other hand, R_t is defined as the value corresponding to Z' when $-Z'' = 0$, which is commonly obtained at intermediate frequencies [56]. The R_p [22, 26] and R_t values have been determined using the following equations derived from the equivalent circuit:

$$\frac{1}{R_p} = \frac{1}{R_1 + R_2} + \frac{1}{R_3} \tag{2}$$

$$R_t = R_1 + R_2 \tag{3}$$

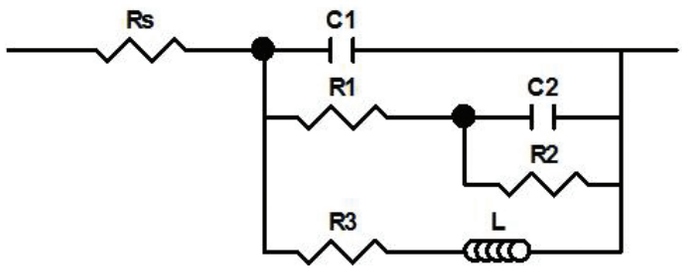

Figure 4. Equivalent circuit used for fitting experimental EIS spectra of the samples.

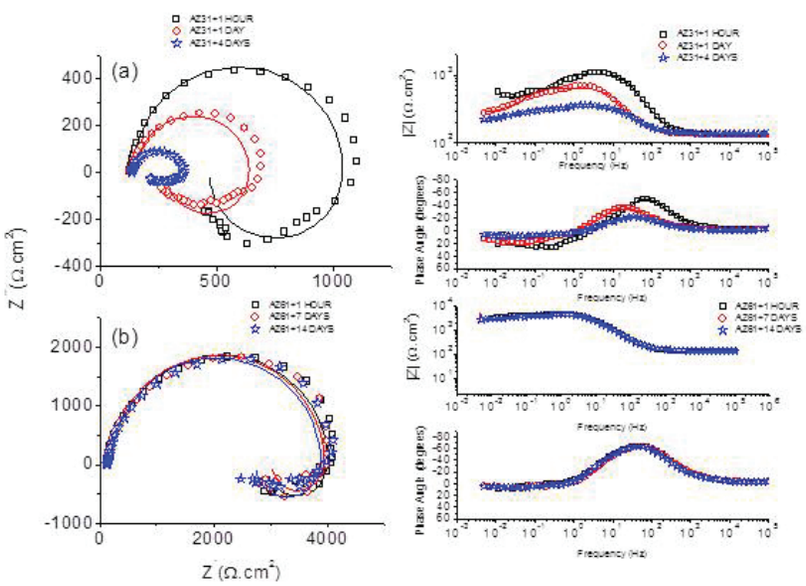

Figure 5. Example of Nyquist and Bode plots with respective fitting for AZ31 and AZ61 alloys with different immersion times in 0.6 M NaCl solution.

http://dx.doi.org/10.5772/65018

The quantitative results from spectra fitting are given in **Tables 3** and **4**, in which the data represent the mean values for the three parallel measurements, and the standard deviation suggests the reproducibility of the EIS measurements.

Immersion time	C_1 (μF cm^{-2})	R_1 (kΩ cm^2)	C_2 (μF cm^{-2})	R_2 (kΩ cm^2)	L (kΩs cm^2)	R_3 (kΩ cm^2)	R_p (kΩ cm^2)	R_t (kΩ cm^2)	I_{H2} (mA cm^{-2})
1 h	5 ± 0.2	0.09 ± 0.03	3 ± 1	0.64 ± 0.15	0.50 ± 0.18	0.41 ± 0.17	0.25 ± 0.09	0.75 ± 0.18	0.13 ± 0.05
4 h	13 ± 6	0.09 ± 0.02	15 ± 12	0.27 ± 0.09	0.26 ± 0.06	0.29 ± 0.12	0.15 ± 0.02	0.37 ± 0.10	0.25 ± 0.01
7 h	16 ± 1	0.12 ± 0.05	20 ± 5	0.31 ± 0.08	0.61 ± 0.19	0.42 ± 0.22	0.21 ± 0.09	0.43 ± 0.13	0.24 ± 0.00
1 day	20 ± 2	0.11 ± 0.02	26 ± 5	0.28 ± 0.10	1.26 ± 0.34	0.19 ± 0.04	0.13 ± 0.03	0.39 ± 0.12	0.25 ± 0.01
2 days	28 ± 2	0.07 ± 0.01	31 ± 6	0.13 ± 0.04	0.61 ± 0.19	0.07 ± 0.01	0.05 ± 0.01	0.20 ± 0.05	0.32 ± 0.01
3 days	25 ± 2	0.08 ± 0.01	45 ± 3	0.11 ± 0.02	0.82 ± 0.10	0.14 ± 0.01	0.08 ± 0.01	0.20 ± 0.03	0.37 ± 0.01
4 days	24 ± 1	0.08 ± 0.01	41 ± 2	0.09 ± 0.01	0.77 ± 0.14	0.14 ± 0.02	0.08 ± 0.01	0.18 ± 0.02	0.40 ± 0.01

Table 3. Fitting results for the EIS measurements performed in 0.6 M NaCl and corrosion current densities obtained from independent measurement of hydrogen evolution for the AZ31 alloy.

Immersion time	C_1 (μF cm^{-2})	R_1 (kΩ cm^2)	C_2 (μF cm^{-2})	R_2 (kΩ cm^2)	L (kΩs cm^2)	R_3 (kΩ cm^2)	R_p (kΩ cm^2)	R_t (kΩ cm^2)	I_{H2} (mA cm^{-2})
1 h	4.18 ± 0.06	1.38 ± 0.02	4.08 ± 0.68	2.16 ± 0.49	43.43 ± 5.63	8.82 ± 1.70	2.53 ± 0.88	3.55 ± 1.82	0.028 ± 0.024
4 h	3.66 ± 0.16	1.25 ± 0.01	2.85 ± 0.08	3.39 ± 0.25	22.58 ± 0.41	16.63 ± 1.94	3.62 ± 0.95	4.64 ± 1.10	0.037 ± 0.005
1 day	3.18 ± 0.05	1.21 ± 0.18	2.25 ± 0.36	4.45 ± 1.32	34.60 ± 5.79	22.72 ± 0.34	4.51 ± 0.72	5.66 ± 1.15	0.034 ± 0.001
2 days	3.20 ± 0.17	1.67 ± 0.18	2.48 ± 0.09	4.31 ± 0.43	61.21 ± 0.54	22.04 ± 1.82	4.70 ± 0.46	5.98 ± 0.61	0.034 ± 0.003
3 days	2.94 ± 0.07	1.02 ± 0.36	2.30 ± 0.60	3.97 ± 0.83	51.80 ± 5.30	18.94 ± 5.40	3.86 ± 0.41	4.92 ± 0.45	0.032 ± 0.003
4 days	3.06 ± 0.04	1.00 ± 0.06	2.20 ± 0.32	3.54 ± 0.59	33.05 ± 2.70	10.66 ± 3.26	3.17 ± 0.55	4.55 ± 0.53	0.030 ± 0.002
7 days	3.03 ± 0.36	0.59 ± 0.21	2.24 ± 0.64	2.96 ± 0.15	31.05 ± 5.96	9.77 ± 0.39	2.60 ± 0.22	3.55 ± 0.36	0.029 ± 0.001
8 days	2.70 ± 0.19	0.33 ± 0.01	2.21 ± 0.17	3.34 ± 0.15	32.45 ± 2.08	8.87 ± 2.39	2.53 ± 0.19	3.68 ± 0.39	0.030 ± 0.000
9 days	2.91 ± 0.31	0.33 ± 0.03	2.34 ± 0.14	3.32 ± 0.19	29.91 ± 3.20	10.16 ± 1.11	2.68 ± 0.04	3.65 ± 0.22	0.030 ± 0.000
10 days	2.94 ± 0.17	0.37 ± 0.16	2.43 ± 0.13	3.53 ± 0.44	25.83 ± 3.79	9.81 ± 0.93	2.65 ± 0.41	3.90 ± 0.25	0.031 ± 0.000
11 days	3.18 ± 0.38	0.42 ± 0.17	2.50 ± 0.08	3.06 ± 0.02	39.67 ± 4.70	7.81 ± 1.29	2.39 ± 0.08	3.47 ± 0.18	0.031 ± 0.000
14 days	3.18 ± 0.35	0.51 ± 0.11	3.09 ± 0.01	3.10 ± 0.30	33.26 ± 2.43	8.43 ± 0.08	2.53 ± 0.11	3.11 ± 0.23	0.033 ± 0.000

Table 4. Fitting results for the EIS measurements performed in 0.6 M NaCl and corrosion current densities obtained from independent measurement of hydrogen evolution for the AZ61 alloy.

The evolution of resistance (R_p and R_t) values as a function of immersion time in 0.6 M NaCl solution is presented in **Figure 6**. After the first day of immersion test, the EIS data for the AZ31 specimen, illustrated in **Figure 6a** and **c** indicate that the resistance (R_p and R_t) values decreased

markedly, approximately consistent with the linear increase in the corrosion current measured by the hydrogen collection presented in **Figure 1**, suggesting that the corrosion product layer formed on this alloy in 0.6 M NaCl is not particularly protective. In contrast, it is interesting to note that there is little effect or a moderate increase observed in the case of the AZ61 specimen over the 14 days immersion time (**Figure 6b** and **d**) in comparison to the high resistance (R_p and R_t) values obtained after 1h of immersion. During the first 2 days of immersion, the AZ61 specimens present a slight increase in the resistance (R_p and R_t) values (**Figure 6b** and **d**), which may be attributed to the growth of partially protective corrosion product film on the surface [30, 57]. According to a previous study [29], filiform corrosion was initiated almost immediately on the magnesium specimens after immersion, and the population of filaments expanded in less than 1 day across the entire exposed surface.

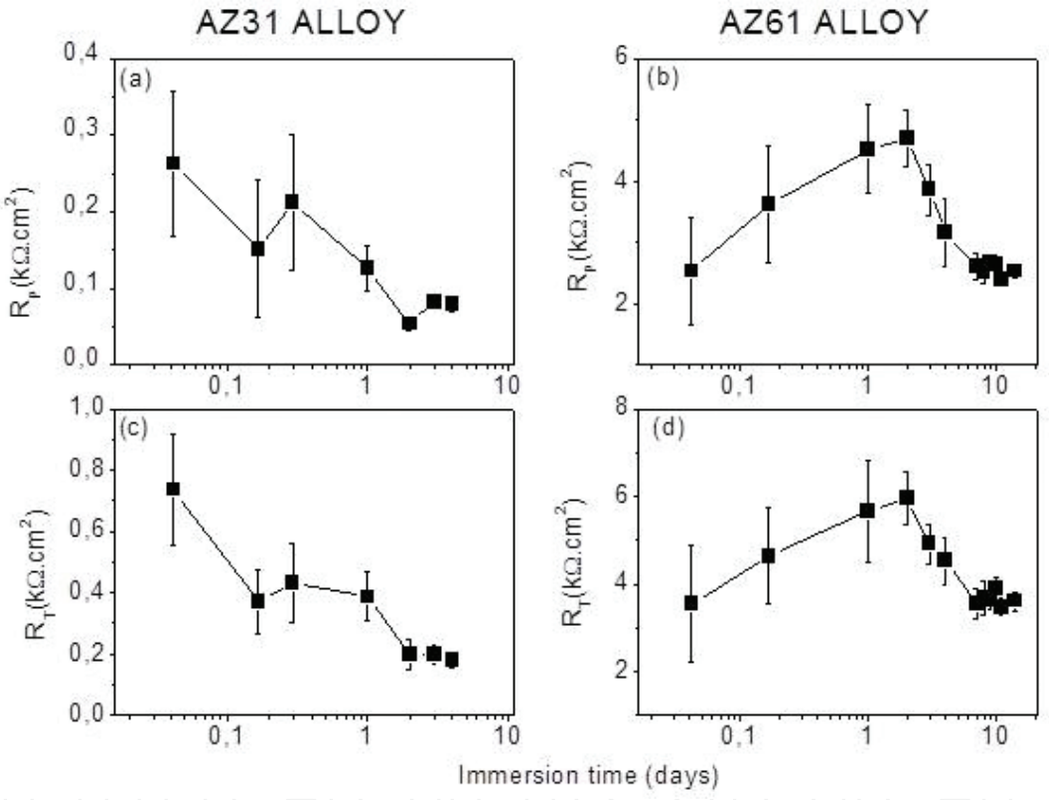

Figure 6. Evolution of the resistance (R_p and R_t) values with immersion time in NaCl 0.6 M solution.

The standard deviations of the average resistance (R_p and R_t) values decrease quickly and strongly with the immersion time indicating the formation of an homogeneous corrosion layer, as it can be seen in **Figure 6**. Curioni et al. [24] observed significant variations in the values of impedance measured under similar conditions attributed to the statistical nature of the corrosion process and to the relatively small electrode size. Because EIS measurements in this study were made with a large (9.0 cm^2) exposed area, it is reasonable to assume that the stochastic nature of the filament formation and growth processes initiated immediately after immersion and expanded in less than 1 day across the entire exposed sur-

face, Samaniego et al. [29] contributed to this initial increase in the deviation of the resistance values. Increasing immersion time showed a decrease in the deviation of the resistance values, probably due to the formation of a uniform corrosion layer on the surface.

3.2. Low-frequency inductive behaviors

As already commented, the impedance diagrams in this study are characterized by a capacitive loop at HF followed by a well-marked inductive loop at LF. Numerous examples of such inductive loops can be found in the literature. An inductive effect may be explained by different reasons. In the corrosion of magnesium and its alloys, the low-frequency inductive loop in the Nyquist plot has been interpreted as a manifestation of localized corrosion damage of the magnesium substrate [58–67], produced by the relaxation of adsorbed species such as Mg(OH)ads+ or $Mg(OH)_2$ [9, 35, 68–73], to the formation and precipitation of a salt film [74, 75], to the incorporation of elements with properties of a semiconductor in the passive films [76] or most recently with accelerated anodic dissolution [22, 77]. However, the species responsible for the inductive response are yet to be determined [22], and the physical interpretation of inductive behavior associated with electrochemical processes is non-trivial, and that is probably the reason why this inductive behavior is often neglected [24].

The notable size of the inductive loops in this work may be seen in **Figure 2**. If the loop size is expressed as the diameter of the semicircle that fits it, and δ is the ratio between the diameters of the inductive and capacitive loops, δ values of the order of 0.6–0.7 have been obtained throughout exposure with the AZ31 alloy but decrease significantly with alloy AZ61 approximately to 0.2–0.3. Our previous EIS data of the specimens corroded under experimental conditions similar to those in this work have produced similar Nyquist plots [8, 15, 27, 28, 29, 49]. Asmussen et al. [77] suggested that the change in EIS behavior seems to be related somehow, with the alloy microstructure and subsequent distribution of the alloying elements, especially Al. According to Song et al. [78], the inductive points could be associated with the corrosion of the α phase while the inert β phase normally shows a capacitive spectrum [79]. **Figure 7** gives the microstructures of the AZ31 and AZ61 magnesium alloys. In the case of AZ61, the electrochemical signals from small amounts of β-phase ($Mg_{17}Al_{12}$), which is formed at the grain boundaries (**Figure 7b**) may modify the α phase formation [78]. In contrast, it can be found that the alloying element Al in the AZ31 alloy completely dissolved into the Mg matrix and no precipitation of the β-phase is observed (**Figure 7a**).

Figure 8 illustrates the relationship between the R_p values and the R_t values obtained from impedance measurements. It is evident that a linear relationship between R_p and R_t values was observed for the two alloys. The absence of significant modifications in the shape of the impedance diagrams throughout the test (**Figure 2**) may explain the high correlation between measured R_p and R_t values. As it has been suggested by Curioni [24], the values of charge transfer resistance (RCT) and corrosion product resistance (RCP) indirectly determine the value of adsorption resistance (RA), and therefore also the zero frequency resistance.

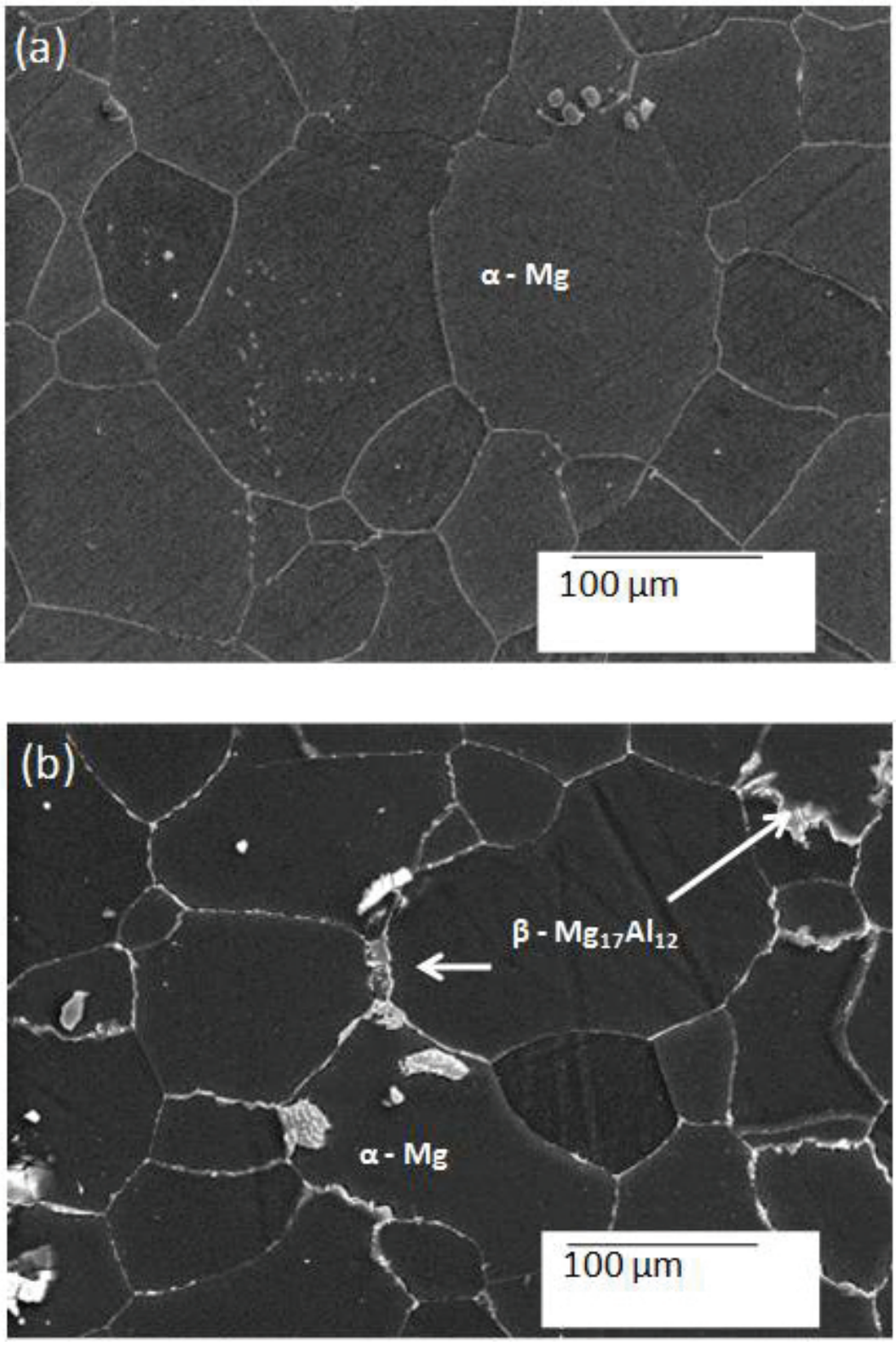

Figure 7. (a) SEM micrographs of AZ31 and (b) AZ61 magnesium alloys.

http://dx.doi.org/10.5772/65018

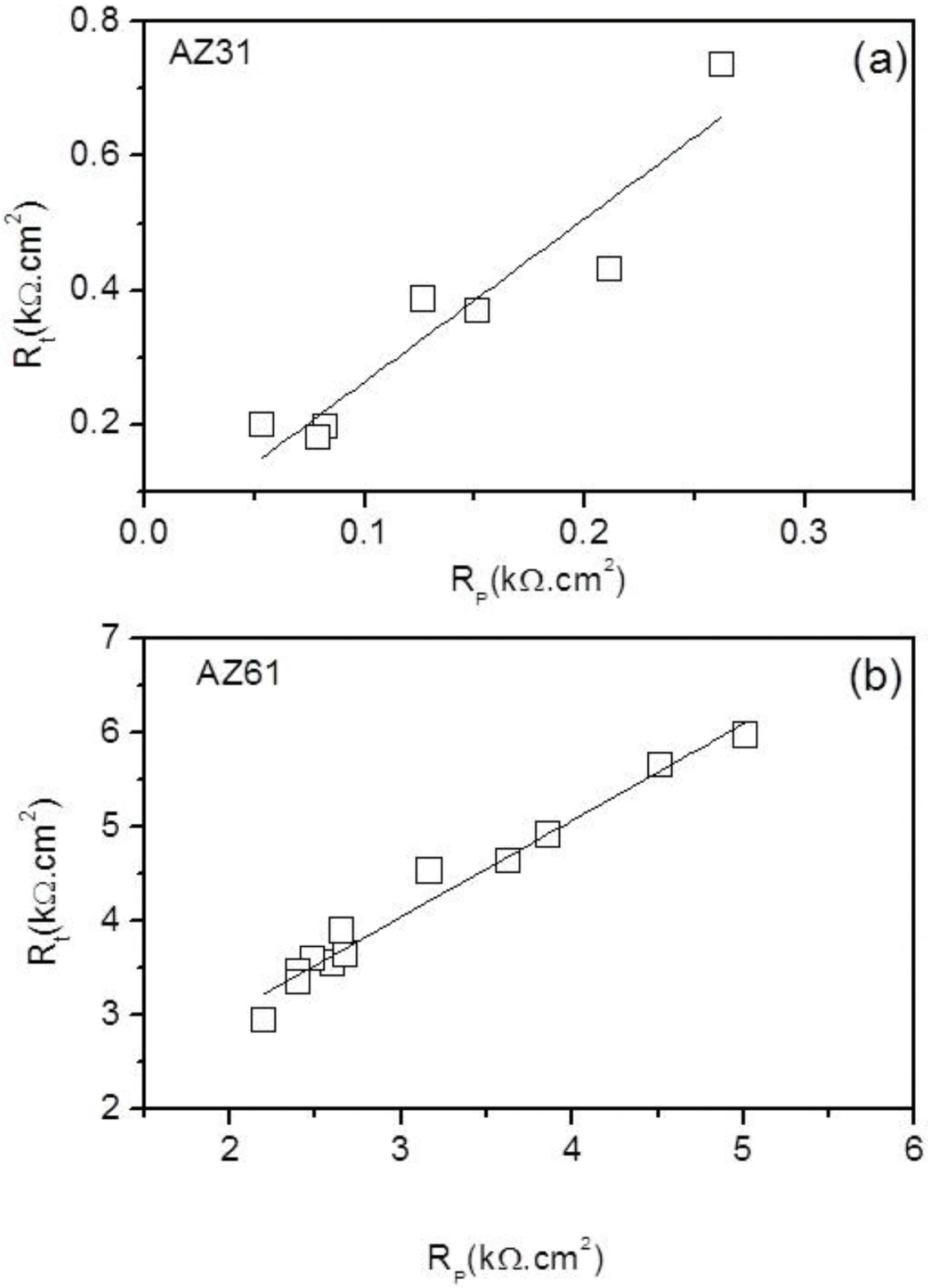

Figure 8. R_t values as a function of R_p values (obtained from **Tables 3** and **4**).

3.3. "Apparent" Stern and Geary values obtained from the correlation between independent EIS and hydrogen evolution measurements

King et al. [22] and Bland et al. [26] have shown that the integration of the corrosion current density over the exposure period *via* Eq. (4), and conversion of the volume of H_2 gas evolved to a corresponding anodic charge ($Q_a^{H_2}$) *via* the ideal gas law and Faraday's Law, all resulted in anodic charge estimations that are similar in value .

$$Q_a^{H_2} = i_{H_2}.t = \int i_{corr}.dt = \int \frac{B}{R}.dt \tag{4}$$

where i_{H_2} is the corrosion current density obtained from hydrogen measurement, i_{corr} is the corrosion current density obtained *via* Eq (1), B is the Stern-Geary coefficient, and R is the value of resistance obtained from fitting of the EIS spectra. In our previous studies [19] and [28], we have also observed high degree of similarity between the amounts of corroded metal determined by hydrogen evolution, gravimetric, and electrochemical measurements.

Under the assumption that B does not change with time for a metal or a metal alloy in a certain aqueous solution [39], one can obtain

$$B' = \frac{Q_a^{H_2}}{\int \left(1/R\right).dt} \tag{5}$$

where B' is the "apparent" Stern-Geary coefficient.

The averages and standard deviations of charge values obtained from hydrogen evolution measurements as a function of time-integrated reciprocal of the polarization resistance R_p or charge transfer resistance R_t values determined by EIS from 1 h and a maximum of 4 days immersion for the AZ31 alloy and 14 days immersion for the AZ61 alloy were used in this study to determine B' values. The results are shown in **Figures 9** and **10**. These figures show that for each alloy immersed in 0.6 M NaCl, charge values from hydrogen evolution measurements and time-integrated reciprocal of the polarization or charge transfer values were approximately proportional. Consequently, the value of B' for that particular system can be directly estimated from the graphs of **Figures 9** and **10** by considering the slope of the fitting lines [24, 39]. A very good correlation between R_p or R_t values estimated by EIS and corrosion currents obtained from independent hydrogen measurements was found. Due to the direct dependence of both resistance values commented above and shown in **Figure 8**, the points in the plots for the determination of the "apparent" Stern-Geary coefficient appear similarly scattered (**Figures 9** and **10**).

http://dx.doi.org/10.5772/65018

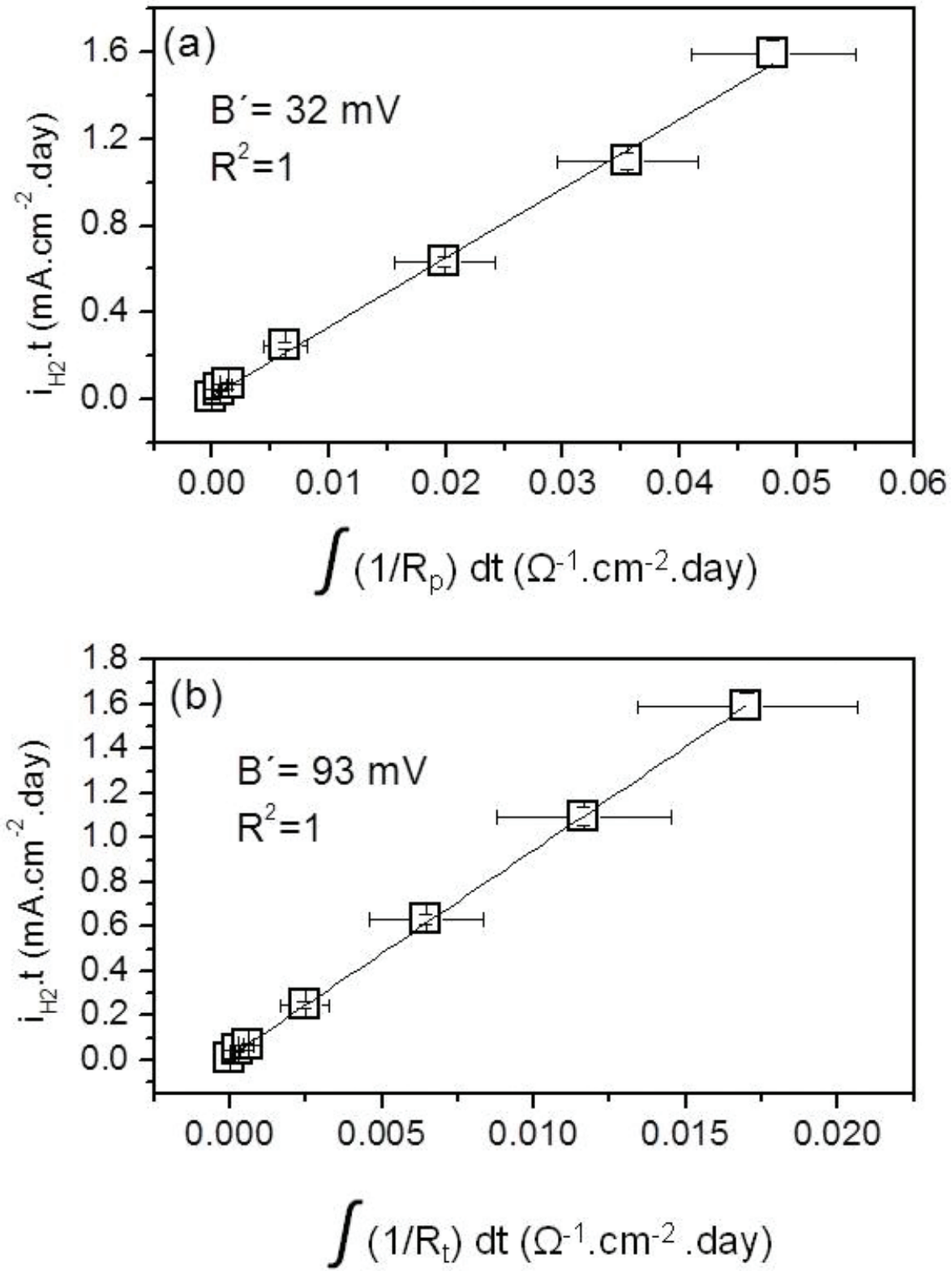

Figure 9. (a) Charge values from hydrogen evolution measurements as a function of time-integrated reciprocal of the polarization resistance R_p or (b) charge transfer resistance R_t values determined by EIS for AZ31 alloy from measurement in 0.6 M NaCl (data from **Table 3**).

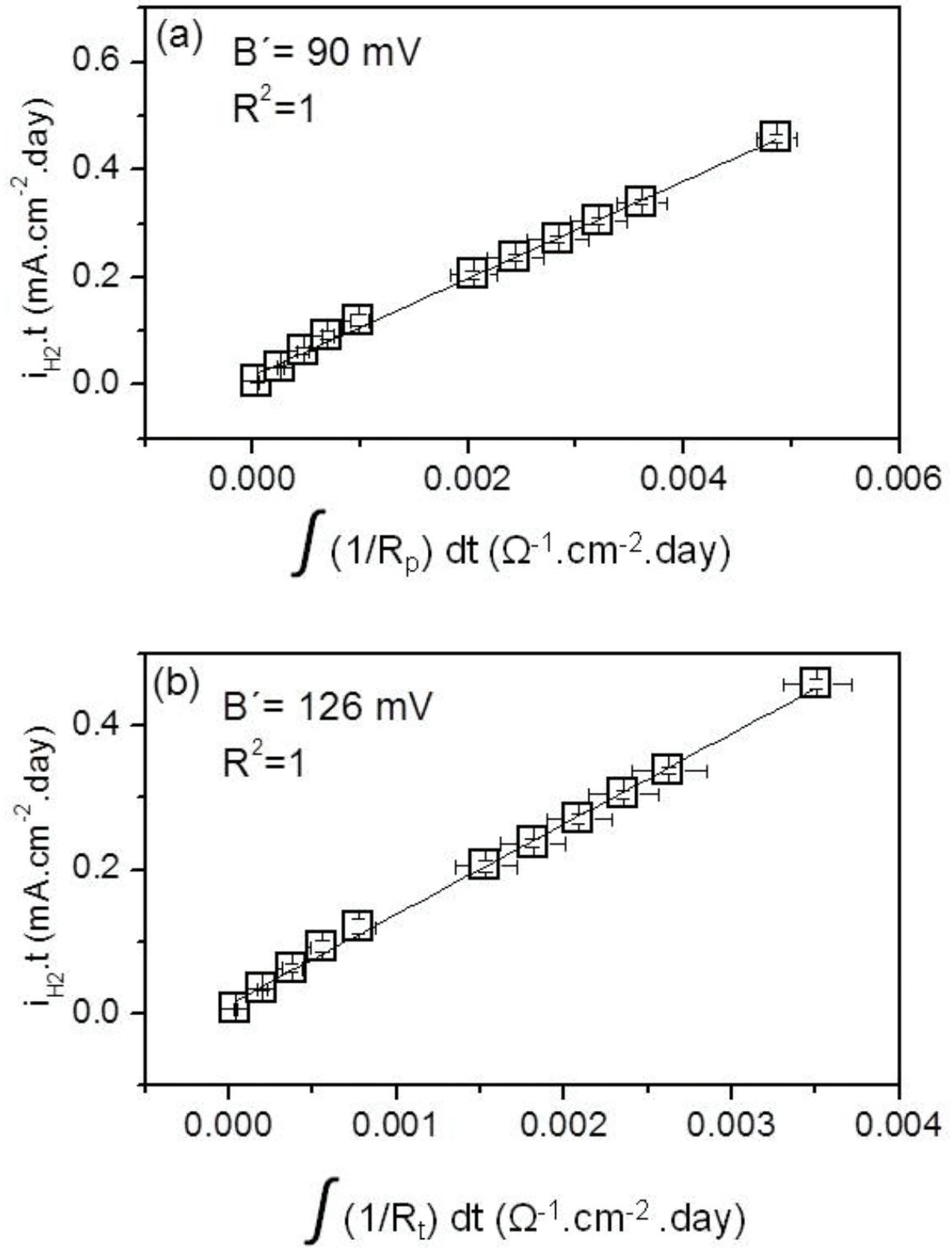

Figure 10. (a) Charge values from hydrogen evolution measurements as a function of time-integrated reciprocal of the polarization resistance R_p or (b) charge transfer resistance R_t values determined by EIS for AZ61 alloy from measurement in 0.6 M NaCl (data from **Table 4**).

Clearly, depending on the resistance and the alloy selected for the calculation, the "apparent" Stern-Geary coefficient is different; 93 or 32 mV for the AZ31 alloy if the charge transfer resistance or the polarization resistance is used and a value of around 126 mV or around 90 mV for the AZ61 alloy if the charge transfer resistance or the polarization resistance is used, respectively. These values are significantly lower compared to the "apparent" Stern-Geary values of 223 mV for the R_t and 116 mV for the R_p previously obtained by Curioni [24] for pure magnesium.

In the case of the AZ31 specimen, the "apparent" Stern-Geary coefficient obtained when the polarization resistance is used is significantly lower (approximately by a factor of 3) compared to when the values of the charge transfer resistance are used (**Figure 8**), while in the case of AZ61 specimen (**Figure 9**), little effect or a moderate decrease in the "apparent" Stern-Geary coefficient is observed. This behavior tends to suggest that the differences between the "apparent" Stern-Geary coefficients obtained from the polarization resistance and charge transfer resistance are dependent on the different sizes of the inductive loops in the impedance diagrams of the studied alloys (**Figure 2**).

A compilation of values of B quoted in the literature of AZ31 and AZ61 alloys arranged by determination method, test solution, time of exposure, author and reference is given in **Table 5**. Quoted B values obtained from Tafel determination method were 5–37 mV for the AZ31 alloy [22, 27, 44, 61, 80–86]. In the literature for AZ61, the *B* values are quoted ranging from 21 to 52 mV [27, 87–91]. The calculated *B*' value of 31 mV for the R_p for the AZ31 alloy is consistent with B values calculated by Bland et al. [26], Cao et al. [44], and Shi et al. [86] (**Table 5**). On the other hand, the *B*' values of around 118 mV for the AZ61 alloy if the charge transfer resistance is similar to that previously obtained by empirical estimation, from electrochemical and gravimetric measurements [27] (**Table 5**).

Alloy	B determination method	Immersion time	B (mV)	NaCl Conc	Author	Ref
AZ31B	Tafel extrapolation method	60 min	7.0	0.6 M	Tekin et al.	[80]
AZ31	Fitting software	48 h	10.1	0.6 M	Lim et al.	[61]
AZ31	Tafel extrapolation method	1800 sg	13.4	0.6 M	Li et al.	[81]
AZ31 Mg alloy	Tafel extrapolation method		16.2	0.6 M	Shen et al.	[82]
Bare AZ31 Mg alloy	Tafel extrapolation method	an initial delay of 5 min	16.5	0.6 M	Einkhah et al.	[83]
AZ31 alloy	Fitting software	30 min of exposure.	17.4	0.6 M	Singh et al.	[84]
AZ31	Fitting software		20.8	0.6 M	Zhang et al	[85]

Alloy	B determination method	Immersion time	B (mV)	NaCl Conc	Author	Ref
AZ31	Tafel assumption	24 h	31.1	0.6 M saturated with Mg(OH)2	Cao et al.	[44]
AZ31	Tafel assumption	24 h	36	0.6 M	King et al.	[22]
AZ31	Tafel assumption	24 h	36.8	0.6 M saturated with Mg(OH)2	Shi et al.	[86]
AZ31	Empirical estimation from electrochemical and gravimetric measurements	10 d	65	0.6 M	Feliu et al.	[27]
Mg6Al	LEV method from polarization curves	for 1 day	21.2	0.6 M saturated with Mg(OH)2	Cao et al.	[87]
Untreated AZ60	Fitting software		21.5	0.6 M	Su et al.	[88]
AZ61 magnesium alloy		30 min immersion	24.2	0.6 M	Rajabalizadeh and Seifzadeh	[91]
AZ61 magnesium alloy		30 min immersion	35.5	0.6 M	Seifzadeh, and Rajabalizadeh	[90]
Heat treated Mg6Al02	LEV method	10 d	38.6	0.6 M saturated with Mg(OH)2	Cao et al.	[91]
Heat treated Mg6Al02	LEV method	10 d	46.1	0.6 M saturated with Mg(OH)2	Cao et al.	[91]
As-cast Mg6Al02	LEV method	10 d	46.7	0.6 M saturated with Mg(OH)2	Cao et al.	[91]
As-cast Mg6Al01	LEV method	10 d	52.4	0.6 M saturated with Mg(OH)2	Cao et al.	[91]
AZ61	Empirical estimation from electrochemical and gravimetric measurements	10 d	120	0.6 M NaCl	Feliu et al.	[27]

Table 5. A selection of B values obtained from the literature.

3.4. Estimation of the corrosion rate from EIS measurements

In **Figure 11**, the variations in EIS-estimated corrosion rate using Eq. (4) and the "apparent" *B'* values obtained in this study with immersion time are compared with the corrosion rate as determined from hydrogen collection. A decrease in the differences between the corrosion rate values derived from impedance measurements and those derived from the hydrogen evolution rate occurs with increasing exposure time. As commented previously, this might be associated with the transformation of an air formed film to the steady corrosion layer for Mg specimens

http://dx.doi.org/10.5772/65018

exposed to saline solutions and the lower hydrogen evolution rates at the beginning of the immersion tests.

Finally, **Figure 12** compares long-term cumulative corrosion rates determined by mass loss, measurement of the H_2 evolved over the entire testing period and integration of the current density (i_{corr}) versus time data determined by the temporal evolution of R_p and R_t over time. All resulted in corrosion rate estimations that are similar in value for each alloy. This corroborating outcome is similar to that from King et al. [22] and Bland et al. [26], indicating that the comparison of unique methods not only provides good comparison for the corrosion rate of magnesium alloys but validates the electrochemical approach as a standalone method.

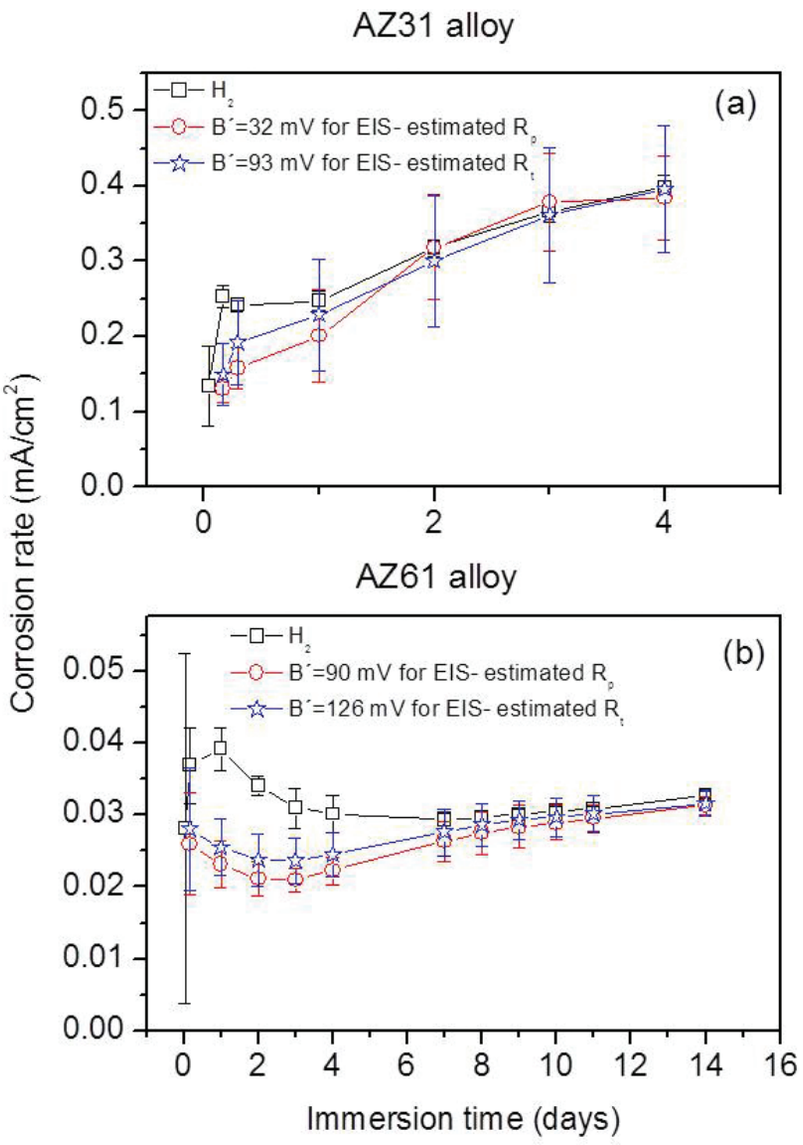

Figure 11. Variation in corrosion rates (mA/cm^2) as a function of immersion time obtained from EIS and hydrogen evolution measurements during 4 days immersion for AZ31 alloy (a) and 14 days of immersion for AZ61 alloy (b) in 0.6 M NaCl.

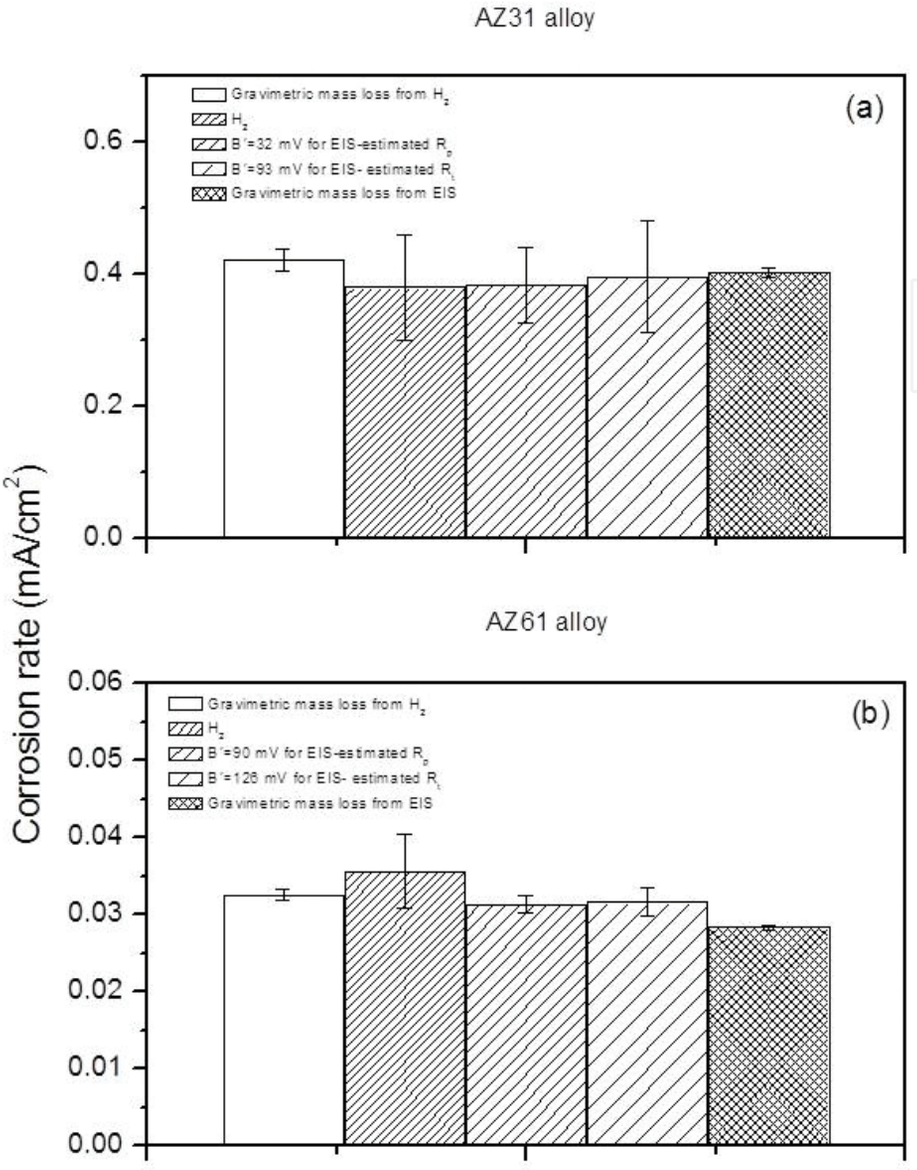

Figure 12. Comparison of corrosion rates (mA/cm^2) obtained from EIS with weight loss and hydrogen evolution measurements after 4 days immersion for AZ31 alloy (a) and 14 days of immersion for AZ61 alloy (a) in 0.6 M NaCl.

4. Conclusions

1. In this research, it has been investigated the possible relationships between independent hydrogen evolution and electrochemical impedance spectroscopy measurements during long-term exposure of AZ31 and AZ61 magnesium alloys in 0.6 M NaCl.

2. Linear relationships with high correlation coefficients have been obtained between time-integrated polarization resistance R_p or charge transfer resistance R_t values determined by EIS and hydrogen evolution measurements.

http://dx.doi.org/10.5772/65018

3. The changes of R_t values with the immersion time have shown a direct and close relationship with the changes of R_p values determined by EIS, being the relationship characteristic of the microstructure of the alloy.

4. With immersion time, the system becomes more stable and the reproducibility of the EIS data appears to be improved. Also, the average error for hydrogen measurements after prolonged periods of exposure is usually smaller.

5. In this investigation, an empirical determination of the "apparent" Stern-Geary coefficient from the correlation between electrochemical and hydrogen measurements has yielded values of around 118 mV for the AZ61 alloy if the charge transfer resistance is used and of around 83 mV if the polarization resistance is used and values of around 97 mV for the AZ31 alloy if the charge transfer resistance is used and of around 31 mV if the polarization resistance is used.

6. No significant errors are obtained in the measurement of the corrosion rate when using R_t or R_p with their corresponding "apparent" Stern-Geary coefficient values.

Acknowledgements

The authors gratefully acknowledge the financial support provided by the Ministry of Economy and Competitiveness of Spain (MAT 2009-13530, MAT2012-30854, and MAT2015-65445-C2-1-R) to carry out the present study, and Prof. S. Feliu is duly acknowledged for fruitful discussions in the frame of this work.

Author details

Maria C. Delgado[1,2], Federico R. García-Galvan[1], Violeta Barranco[1] and Sebastian Feliu Batlle[1*]

*Address all correspondence to: sfeliu@cenim.csic.es

1 National Centre for Metallurgical Research (CENIM-CSIC), Madrid, Spain

2 Department of Materials Science, Simon Bolivar University, Baruta, Venezuela

References

[1] Gray JE, Luan B. Protective coatings on magnesium and its alloys – a critical review. Journal of Alloys and Compounds. 2002; 336: 88–113. DOI: 10.1016/S0925-8388(01)01899-0

[2] Kulekci MK. Magnesium and its alloys applications in automotive industry. International Journal of Advanced Manufacturing Technology. 2008; 39: 851–865. DOI: 10.1007/s00170-007-1279-2

[3] Witte F, Hort N, Vogt C, Cohen S, Kainer KU, Willumeit R, Feyerabend F. Degradable biomaterials based on magnesium corrosion. Current Opinion in Solid State and Materials Science. 2008; 12: 63–72. DOI: 10.1016/j.cossms.2009.04.001

[4] Song GL. Recent progress in corrosion and protection of magnesium alloys. Advanced Engineering Materials. 2005; 7: 563–586. DOI: 10.1002/adem.200500013

[5] Shkirskiy V, King AD, Gharbi O, Volovitch P, Scully JR, Ogle K, Birbilis N. Revisiting the electrochemical impedance spectroscopy of magnesium with online inductively coupled plasma atomic emission spectroscopy. ChemPhysChem. 2015; 16: 536–539. DOI: 10.1002/cphc.201402666

[6] Banerjee PC, Raman RKS, Durandet Y, McAdam G. Electrochemical investigation of the influence of laser surface melting on the microstructure and corrosion behaviour of ZE41 magnesium alloy – an EIS based study. Corrosion Science. 2011; 53: 1505–1514. DOI: 10.1016/j.corsci.2011.01.017

[7] Feliu Jr. S, Barajas R, Bastidas JM, Morcillo M, Feliu S. Study of protection mechanisms of zinc-rich paints by electrochemical impedance spectroscopy. In: Scully JR, Silverman DC, Kendig MW, editors. Electrochemical Impedance: Analysis and Interpretation. Vol. 1188. Philadelphia: ASTM; 1993. pp. 438–449. DOI: 10.1520/STP18084S

[8] Feliu Jr. S, Maffiotte C, Samaniego A, Galvan JC, Barranco V. Effect of naturally formed oxide films and other variables in the early stages of Mg-alloy corrosion in NaCl solution. Electrochimica Acta. 2011; 56: 4454–4565. DOI: 10.1016/j.electacta.2011.02.077

[9] Jamesh M, Kumar S, Sankara Narayanan TSNS. Corrosion behavior of commercially pure Mg and ZM21 Mg alloy in Ringer's solution – Long term evaluation by EIS. Corrosion Science. 2011; 53: 645–654. DOI: 10.1016/j.corsci.2010.10.011

[10] Jian SY, Chu YR, Lin CS. Permanganate conversion coating on AZ31 magnesium alloys with enhanced corrosion resistance. Corrosion Science. 2015; 93: 301–309. DOI: 10.1016/j.corsci.2015.01.040

[11] Rocca E, Juers C, Steinmetz J. Corrosion behaviour of chemical conversion treatments on as-cast Mg–Al alloys: Electrochemical and non-electrochemical methods. Corrosion Science. 2010; 52: 2172–2178. DOI: 10.1016/j.corsci.2010.02.036

[12] Ardelean H, Frateur I, Marcus P. Corrosion protection of magnesium alloys by cerium, zirconium and niobium-based conversion coatings. Corrosion Science. 2008; 50: 1907–1918. DOI: 10.1016/j.corsci.2008.03.015

[13] Chu YR, Lin CS. Citrate gel conversion coating on AZ31 magnesium alloys. Corrosion Science. 2014; 87: 288–296. DOI: 10.1016/j.corsci.2014.06.034

[14] Chen J, Song YW, Shan DY, Han EH. Study of the corrosion mechanism of the *in situ* grown Mg–Al–CO32- hydrotalcite film on AZ31 alloy. Corrosion Science. 2012; 65: 268–277. DOI: 10.1016/j.corsci.2012.08.026

[15] Feliu Jr. S, Samaniego A, Barranco V, El-Hadad AA, Llorente I, Adeva P. The effect of low temperature heat treatment on surface chemistry and corrosion resistance of commercial magnesium alloys AZ31 and AZ61 in 0.6 M NaCl solution. Corrosion Science. 2014; 80: 461–472. DOI: 10.1016/j.corsci.2013.11.065

[16] Pebere N, Riera C, Dabosi F. Investigation of magnesium corrosion in aerated sodium-sulfate solution by electrochemical impedance spectroscopy. Electrochimica Acta. 1990; 35: 555–561. DOI: 10.1016/0013-4686(90)87043-2

[17] Makar L, Kruger J. Corrosion studies of rapidly solidified magnesium alloys. Journal of the Electrochemical Society 1990; 137: 414–421. DOI: 10.1149/1.2086455

[18] Mathieu S, Rapin C, Hazan J, Steinmetz P. Corrosion behaviour of high pressure die-cast and semi-solid cast AZ91D alloys. Corrosion Science. 2002; 44: 2737–2756. DOI: 10.1016/S0010-938X(02)00075-6

[19] Feliu Jr. S, Samaniego A, Barranco V, El-Hadad AA, Llorente I, Serra C, Galvan JC. A study on the relationships between corrosion properties and chemistry of thermally oxidised surface films formed on polished commercial magnesium alloys AZ31 and AZ61. Applied Surface Science. 2014; 295: 219–230. DOI: 10.1016/j.apsusc.2014.01.033

[20] Feliu Jr. S, Samaniego A, Bermudez EA, El-Hadad AA, Llorente I, Galvan JC. Effect of native oxide film on commercial magnesium alloys substrates and carbonate conversion coating growth and corrosion resistance. Materials. 2014; 7: 2534–2560. DOI: 10.3390/ma7042534

[21] Stern M, Geary AL. Electrochemical polarization 1. A theoretical analysis of the shape of polarization curves. Journal of the Electrochemical Society. 1957; 104: 56–63. DOI: 10.1149/1.2428496

[22] King AD, Birbilis N, Scully JR. Accurate electrochemical measurement of magnesium corrosion rates; a combined impedance, mass-loss and hydrogen collection study. Electrochimica Acta. 2014; 121: 394–406. DOI: 10.1016/j.electacta.2013.12.124

[23] Poursaee A. Potentiostatic transient technique, a simple approach to estimate the corrosion current density and Stern–Geary constant of reinforcing steel in concrete. Cement and Concrete Research. 2010; 40: 1451–1458. DOI: 10.1016/j.cemconres.2010.04.006

[24] Curioni M, Scenini F, Monetta T, Bellucci F. Correlation between electrochemical impedance measurements and corrosion rate of magnesium investigated by real-time hydrogen measurement and optical imaging. Electrochimica Acta. 2015; 166: 372–384. DOI: 10.1016/j.electacta.2015.03.050

[25] Fajardo S, Frankel GS. Gravimetric method for hydrogen evolution measurements on dissolving magnesium. Journal of the Electrochemical Society. 2015; 162: C693–C701. DOI: 10.1149/2.0241514jes

[26] Bland LG, King AD, Birbilis N, Scully JR. Assessing the corrosion of commercially pure magnesium and commercial AZ31B by electrochemical impedance, mass-loss, hydrogen collection, and inductively coupled plasma optical emission spectrometry solution analysis. Corrosion. 2015; 71: 128–145. DOI: 10.5006/1419

[27] Feliu Jr. S, Maffiotte C, Samaniego A, Galván JC, Barranco V. Effect of the chemistry and structure of the native oxide surface film on the corrosion properties of commercial AZ31 and AZ61 alloys. Applied Surface Science. 2011; 257: 8558–8568. DOI: 10.1016/j.apsusc.2011.05.014

[28] Feliu Jr. S, Llorente I. Corrosion product layers on magnesium alloys AZ31 and AZ61: Surface chemistry and protective ability. Applied Surface Science. 2015; 347: 736–746. DOI: 10.1016/j.apsusc.2015.04.189

[29] Samaniego A, Llorente I, Feliu Jr. S. Combined effect of composition and surface condition on corrosion behavior of magnesium alloys AZ31 and AZ61. Corrosion Science. 2013; 68: 66–71. DOI: 10.1016/j.corsci.2012.10.034

[30] Feliu Jr. S, Maffiotte C, Galvan JC, Barranco V. Atmospheric corrosion of magnesium alloys AZ31 and AZ61 under continuous condensation conditions. Corrosion Science. 2011; 53: 1865–1872. DOI: 10.1016/j.corsci.2011.02.003

[31] Samaniego A, Feliu Jr. S. Different performance of factors affecting the estimation of the corrosion rate in magnesium alloys by implementation of the common methods for electrochemical measurements. In: Monteiro WA, editor. Light Metal Alloys Applications. Croatia: Intech; 2014. p. 145–161. DOI: 10.5772/58370

[32] Atrens A, Song GL, Liu M, Shi Z, Cao F, Dargusch MS. Review of recent developments in the field of magnesium corrosion. Advanced Engineering Materials. 2015; 17: 400–453. DOI:10.1002/adem.201400434

[33] Abidin NIZ, Rolfe B, Owen H, Malisano J, Martin D, Hofstetter J, Uggowitzer PJ, Atrens A. The in vivo and in vitro corrosion of high-purity magnesium and magnesium alloys WZ21 and AZ91. Corrosion Science. 2013; 75: 354–366. DOI: 10.1016/j.corsci.2013.06.019

[34] Abidin NIZ, Atrens AD, Martin D, Atrens A. Corrosion of high purity Mg, $Mg_2Zn_{0.2}Mn$, ZE41 and AZ91 in Hank's solution at 37°C. Corrosion Science. 2011; 53: 3542–3556. DOI: 10.1016/j.corsci.2011.06.030

[35] Song GL, Song SZ. A possible biodegradable magnesium implant material. Advanced Engineering Materials. 2007; 9: 298–302. DOI: 10.1002/adem.200600252

[36] Song GL. Control of biodegradation of biocompatible magnesium alloys. Corrosion Science. 2007; 49: 1696–1701. DOI: 10.1016/j.corsci.2007.01.001

[37] Wang H, Estrin Y, Fu H, Song G, Zuberova Z. The effect of pre-processing and grain structure on the bio-corrosion and fatigue resistance of magnesium alloy AZ31. Advanced Engineering Materials. 2007; 9: 967–972. DOI: 10.1002/adem.200700200

[38] Atrens A, Song GL, Cao F, Shi Z, Bowen PK. Advances in Mg corrosion and research suggestions. Journal of Magnesium and Alloys. 2013; 1: 177–200. DOI: 10.1016/j.jma.2013.09.003

[39] Hsieh MK, Dzombak DA, Vidie RD. Bridging gravimetric and electrochemical approaches to determine the corrosion rate of metals and metal alloys in cooling systems: Bench scale evaluation method. Industrial and Engineering Chemistry Research. 2010; 49: 9117–9123. DOI: 10.1021/ie100217k

[40] Kirkland NT, Birbilis N, Staiger MP. Assessing the corrosion of biodegradable magnesium implants: A critical review of current methodologies and their limitations. Acta Biomaterialia. 2012; 8: 925–936. DOI: 10.1016/j.actbio.2011.11.014

[41] Liu M, Schmutz P, Uggowitzer PJ, Song GL, Atrens A. The influence of yttrium (Y) on the corrosion of Mg-Y binary alloys. Corrosion Science. 2010; 52: 3687–3701. DOI: 10.1016/j.corsci.2010.07.019

[42] Qiao ZX, Shi ZM, Hort N, Abidin NIZ, Atrens A. Corrosion behaviour of a nominally high purity Mg ingot produced by permanent mould direct chill casting. Corrosion Science. 2012; 61: 185–207. DOI: 10.1016/j.corsci.2012.04.030

[43] Shi ZM, Cao FY, Song GL, Atrens A. Low apparent valence of Mg during corrosion. Corrosion Science. 2014; 88: 434–443. DOI: 10.1016/j.corsci.2014.07.060

[44] Shi ZM, Liu M, Atrens A. Measurement of the corrosion rate of magnesium alloys using Tafel extrapolation. Corrosion Science. 2010; 52: 579–588. DOI: 10.1016/j.corsci.2009.10.016

[45] Cao FY, Shi ZM, Hofstetter J, Uggowitzer PJ, Song GL, Liu M, Atrens A. Corrosion of ultra-high-purity Mg in 3.5% NaCl solution saturated with Mg(OH)2. Corrosion Science. 2013; 75: 78–99. DOI: 10.1016/j.corsci.2013.05.018

[46] Frankel GS, Samaniego A, Birbilis N. Evolution of hydrogen at dissolving magnesium surfaces. Corrosion Science. 2013; 70: 104–111. DOI: 10.1016/j.corsci.2013.01.017

[47] ZView software. Version 3.4d (Scribner Associates Inc.), Southern Pines, NC, USA.

[48] Johnston S, Shi ZM, Atrens A. The influence of pH on the corrosion rate of high-purity Mg, AZ91 and ZE41 in bicarbonate buffered Hanks' solution. Corrosion Science. 2015; 101: 182–192. DOI: 10.1016/j.corsci.2015.09.018

[49] Feliu Jr. S, El-Hadad AA, Barranco V, Llorente I, García-Galván FR, Jiménez-Morales A, Galván JC. Native oxide films on AZ31 and AZ61 commercial magnesium alloys: Corrosion behaviour, effect on isothermal oxidation and sol–gel thin film formation.

In: Ahmad Z, editor. New Trends in Alloy Development, Characterization and Application. Croatia: Intech; 2015. p. 97–122. DOI: 10.5772/60721

[50] Zander D, Schnatterer C. The influence of manufacturing processes on the microstructure and corrosion of the AZ91D magnesium alloy evaluated using a computational image analysis. Corrosion Science. 2015; 98: 291–303. DOI: 10.1016/j.corsci.2015.05.032

[51] Lebouil S, Duboin A, Monti F, Tabeling P, Volovitch P, Ogle K. A novel approach to online measurement of gas evolution kinetics: Application to the negative difference effect of Mg in chloride solution. Electrochimica Acta. 2014; 124: 176–182. DOI: 10.1016/j.electacta.2013.07.131

[52] Fajardo S, Frankel GS. Effect of impurities on the enhanced catalytic activity for hydrogen evolution in high purity magnesium. Electrochimica Acta. 2015; 165: 255–267. DOI: 10.1016/j.electacta.2015.03.021

[53] Murray JN, Moran PJ, Gileadi E. Utilization of the specific pseudocapacitance for determination of the area of corroding steel surfaces. Corrosion. 1988; 44: 533–538.

[54] Brooks EK, Der S, Ehrensberger MT. Corrosion and mechanical performance of AZ91 exposed to simulated inflammatory conditions. Materials Science and Engineering: C. 2016; 60: 427–436. DOI: 10.1016/j.msec.2015.11.059

[55] Wang J, Jang Y, Wan GJ, Giridharan V, Song GL, Xu ZG, Koo Y, Qi PK, Sankar J, Huang N, Yun YH. Flow-induced corrosion of absorbable magnesium alloy: *In-situ* and real-time electrochemical study. Corrosion Science. 2016; 104: 277–289. DOI: 10.1016/j.corsci.2015.12.020s

[56] Yeganeh M, Saremi M. Corrosion inhibition of magnesium using biocompatible Alkyd coatings incorporated by mesoporous silica nanocontainers. Progress in Organic Coatings. 2015; 79: 25–30. DOI: 10.1016/j.porgcoat.2014.10.015

[57] Hou RQ, Ye CQ, Chen CD, Dong SG, Lv MQ, Zhang S, Pan JS, Song GL, Lin CJ. Localized corrosion of binary Mg–Ca alloy in 0.9 wt% sodium chloride solution. Acta Metallurgica Sinica (English Letters). 2016; 29: 46–57. DOI: 10.1007/s40195-015-0361-2

[58] Wu CS, Zhang Z, Cao FH, Zhang LJ, Zhang JQ, Cao CN. Study on the anodizing of AZ31 magnesium alloys in alkaline borate solutions. Applied Surface Science. 2007; 253: 3893–3898. DOI: 10.1016/j.apsusc.2006.08.020

[59] Metikos-Hukovic M, Babic R, Grubac Z, Brinic S. Impedance spectroscopic study of aluminum and Al-alloys in acid-solution – inhibitory-action of nitrogen-containing compounds. Journal of Applied Electrochemistry. 1994; 24: 772–778. DOI: 10.1007/BF00578093

[60] Song YW, Shan DY, Chen RS, Han EH. Corrosion characterization of Mg–8Li alloy in NaCl solution. Corrosion Science. 2009; 51: 1087–1094. DOI: 10.1016/j.corsci.2009.03.011

[61] Liang J, Srinivasan PB, Blawert C, Dietzel W. Influence of pH on the deterioration of plasma electrolytic oxidation coated AM50 magnesium alloy in NaCl solutions. Corrosion Science 2010; 52: 540–547. DOI: 10.1016/j.corsci.2009.10.011

[62] Zhang YJ, Yan CW, Wang FH, Li WF. Electrochemical behavior of anodized Mg alloy AZ91D in chloride containing aqueous solution. Corrosion Science. 2005; 47: 2816–2831. DOI: 10.1016/j.corsci.2005.01.010

[63] Kannan MB. Influence of microstructure on the *in vitro* degradation behaviour of magnesium alloys. Materials Letters. 2010; 64: 739–742. DOI: 10.1016/j.matlet.2010.01.022

[64] Jin S, Amira S, Ghali E. Electrochemical impedance spectroscopy evaluation of the corrosion behavior of die cast and thixocast AXJ530 magnesium alloy in chloride solution. Advanced Engineering Materials. 2007; 9: 75–83. DOI: 10.1002/adem.200600199

[65] Alvarez-Lopez M, Pereda MD, del Valle JA, Fernandez-Lorenzo M, Garcia-Alonso MC, Ruano OA, Escudero ML. Corrosion behaviour of AZ31 magnesium alloy with different grain sizes in simulated biological fluids. Acta Biomaterialia. 2010; 6: 1763–1771. DOI: 10.1016/j.actbio.2009.04.041

[66] Srinivasan PB, Liang J, Balajeee RG, Blawert C, Stormer M, Dietzel W. Effect of pulse frequency on the microstructure, phase composition and corrosion performance of a phosphate-based plasma electrolytic oxidation coated AM50 magnesium alloy. Applied Surface Science. 2010; 256: 3928–3935. DOI: 10.1016/j.apsusc.2010.01.052

[67] Lim TS, Ryu HS, Hong SH. Electrochemical corrosion properties of CeO_2-containing coatings on AZ31 magnesium alloys prepared by plasma electrolytic oxidation. Corrosion Science. 2012; 62: 104–111. DOI: 10.1016/j.corsci.2012.04.043

[68] Baril G, Blanc C, Pebere N. AC impedance spectroscopy in characterizing time-dependent corrosion of AZ91 and AM50 magnesium alloys: Characterization with respect to their microstructures. Journal of the Electrochemical Society. 2001; 148: b469–b496. DOI: 10.1149/1.1415722

[69] Baril G, Galicia G, Deslouis C, Pebere N, Tribollet B, Vivier V. An impedance investigation of the mechanism of pure magnesium corrosion in sodium sulfate solutions. Journal of the Electrochemical Society. 2007; 154: C108–C113. DOI: 10.1149/1.2401056

[70] Chang JW, Guo XW, Fu PH, Peng LM, Ding WJ. Effect of heat treatment on corrosion and electrochemical behaviour of Mg–3Nd–0.2Zn–0.4Zr (wt.%) alloy. Electrochimica Acta. 2007; 52: 3160–3167. DOI: 10.1016/j.electacta.2006.09.069

[71] Brett CMA, Dias L, Trindade B, Fischer R, Mies S. Characterisation by EIS of ternary Mg alloys synthesised by mechanical alloying. Electrochimica Acta. 2006; 51: 1752–1760. DOI: 10.1016/j.electacta.2005.02.124

[72] Chang JW, Guo XW, He SM, Fu PH, Peng LM, Ding WJ. Investigation of the corrosion for Mg–xGd–3Y–0.4Zr (x = 6, 8, 10, 12 wt%) alloys in a peak-aged condition. Corrosion Science. 2008; 50: 166–177. DOI: 10.1016/j.corsci.2007.06.003

[73] Turhan MC, Lynch R, Killian MS, Virtanen S. Effect of acidic etching and fluoride treatment on corrosion performance in Mg alloy AZ91D (MgAlZn). Electrochimica Acta. 2009; 55: 250–257. DOI: 10.1016/j.electacta.2009.08.046

[74] Breslin CB, Rudd AL. Activation of pure Al in an indium-containing electrolyte — an electrochemical noise and impedance study. Corrosion Science. 2000; 42:1023–1039. DOI: 10.1016/S0010-938X(99)00128-6

[75] Barbucci A, Bruzzone G, Delucchi M, Panizza M, Cerisola G. Breakdown of passivity of aluminium alloys by intermetallic phases in neutral chloride solution. Intermetallics. 2000; 8: 305–312. DOI: 10.1016/S0966-9795(99)00114-4

[76] He WW, Zhang EL, Yang K. Effect of Y on the bio-corrosion behavior of extruded Mg–Zn–Mn alloy in Hank's solution. Materials Science and Engineering: C. 2010; 30: 167–174. DOI: 10.1016/j.msec.2009.09.014

[77] Asmussen RM, Binns WJ, Jakupi P, Shoesmith D. Microstructural effects on corrosion of AM50 magnesium alloys. Journal of the Electrochemical Society. 2014; 161: C501–C508. DOI: 10.1149/2.0781410jes

[78] Song GL, Bowles AL, St John DH. Corrosion resistance of aged die cast magnesium alloy AZ91D. Materials Science and Engineering: A. 2004; 366: 74–86. DOI: 10.1016/j.msea.2003.08.060

[79] Song GL, Atrens A, Wu XL, Zhang B. Corrosion behaviour of AZ21, AZ501 and AZ91 in sodium chloride. Corrosion Science. 1998; 40: 1769–1791. DOI: 10.1016/S0010-938X(98)00078-X

[80] Tekin KC, Malayoglu U, Shrestha S. Electrochemical behavior of plasma electrolytic oxide coatings on rare earth element containing Mg alloys. Surface and Coatings Technology. 2013; 236: 540–549. DOI: 10.1016/j.surfcoat.2013.10.051

[81] Lim TS, Ryu HS, Hong SH. Electrochemical corrosion properties of CeO2-containing coatings on AZ31 magnesium alloys prepared by plasma electrolytic oxidation. Corrosion Science 2012; 62: 104–111. DOI: 10.1016/j.corsci.2012.04.043

[82] Shen DJ, Ma HJ, Guo CH, Cai JR, Li GL, He DL, Yang QX. Effect of cerium and lanthanum additives on plasma electrolytic oxidation of AZ31 magnesium alloy. Journal of Rare Earths. 2013; 31: 1208–1213. DOI: 10.1016/S1002-0721(12)60428-1

[83] Einkhah F, Lee KM, Sani MAF, Yoo B, Shin DH. Structure and corrosion behavior of oxide layer with Zr compounds on AZ31 Mg alloy processed by two-step plasma electrolytic oxidation. Surface and Coatings Technology. 2014; 238: 75–79. DOI: 10.1016/j.surfcoat.2013.10.042

[84] Singh IB, Singh M, Das S. A comparative corrosion behavior of Mg, AZ31 and AZ91 alloys in 3.5% NaCl solution. Journal of Magnesium and Alloys. 2015; 3: 142–148. DOI: 10.1016/j.jma.2015.02.004

[85] Zhang JF, Yan CW, Wang FH. Electrodeposition of Al–Mn alloy on AZ31B magnesium alloy in molten salts. Applied Surface Science. 2009; 255: 4926–4932. DOI: 10.1016/j.apsusc.2008.12.039

[86] Shi ZM, Cao FY, Song GL, Liu M, Atrens A. Corrosion behaviour in salt spray and in 3.5% NaCl solution saturated with $Mg(OH)_2$ of as-cast and solution heat-treated binary Mg–RE alloys: RE = Ce, La, Nd, Y, Gd. Corrosion Science. 2013; 76: 98–118. DOI: 10.1016/j.corsci.2013.06.032

[87] Cao FY, Shi ZM, Song GL, Liu M, Dargusch MS, Atrens A. Influence of hot rolling on the corrosion behavior of several Mg–X alloys. Corrosion Science. 2015; 90: 176–191. DOI: 10.1016/j.corsci.2014.10.012

[88] Su YC, Li GY, Lian JS. A chemical conversion hydroxyapatite coating on AZ60 magnesium alloy and its electrochemical corrosion behaviour. International Journal of Electrochemical Science. 2012; 7: 11497–11511.

[89] Rajabalizadeh Z, Seifzadeh D. The effect of copper ion on microstructure, plating rate and anticorrosive performance of electroless Ni-P coating on AZ61 magnesium alloy. Protection of Metals and Physical Chemistry of Surfaces. 2014; 50: 516–523. DOI: 10.1134/S2070205114040157

[90] Rajabalizadeh Z, Seifzadeh D. Environmentally-friendly method for electroless Ni–P plating on magnesium alloy. Surface and Coatings Technology. 2013; 218: 119–126. DOI: 10.1016/j.surfcoat.2012.12.039

[91] Cao FY, Shi ZM, Song GL, Liu M, Atrens A. Corrosion behaviour in salt spray and in 3.5% NaCl solution saturated with Mg(OH)2 of as-cast and solution heat-treated binary Mg–X alloys: X = Mn, Sn, Ca, Zn, Al, Zr, Si, Sr. Corrosion Science. 2013; 76: 60–97. DOI: 10.1016/j.corsci.2013.06.030

IntechOpen